Attitude control for a tiltwing aircraft under tail actuator failures

D. Schatten* and D. Moormann
RWTH Aachen University, Templergraben 55, 52062 Aachen, Germany

ABSTRACT

In this paper we present a concept for attitude control of a tilt wing aircraft under tail rotor failures. During hover flight, the exampled tilt wing aircraft flies as a conventional tri-copter with two main motors and one auxiliary tail rotor. In case of an tail rotor failure the body swings beneath the main wing and the aircraft stabilizes as a flying wing. Using a body-fixed coordinate system, angular accelerations are controlled by a robust attitude controller on the basis of Nonlinear Dynamic Inversion (INDI). Combined with a height controller and an LQR based angular acceleration controller, a controlled flight and descend can be achieved.

1 INTRODUCTION

The combination of vertical take-off and landing (VTOL) capabilities with the ability to fly as conventional airplanes, make tilt wing aircraft a versatile design. While at cruising speed, the tilt wing aircraft uses its main wing to generate lift. During VTOL the aircraft rotates its main wing upwards and the main engines thrust is used to climb and hover. To stabilize and enable pitching maneuvers during hover, an auxiliary tail rotor is employed. During this VTOL phase, engine failures lead to uncontrolled descend if not compensated by an emergency maneuver or redundant engine designs [1] [2] [3] Redundant engine design concepts, like including more engines than needed for thrust generation always have the negative downside that as the overall system mass increases and therefore payload or flight time is reduced. To address this problem, emergency maneuvers can be employed. While in fast forward flight, classical one engine out procedures can be applied [1] . However, engine failures in hover flight pose a critical flight situation due to the lack of thrust generation and limited recovery altitude. In this paper we present a control structure which enables an unmanned tilt wing aircraft to safely control its attitude while maintaining its altitude during tail rotor failure. Taking into consideration that the motor thrust in combination with the tilt angle affects pitch momentum as well as the longitudinal acceleration, a prioritization for the stability around pitch axis while maintaining altitude is favorable.

*Email address(es): schatten@fsd.rwth-aachen.de

2 MODEL

The aircraft which is being stabilized is depicted in figure 1. This tilt wing has a span of 1.5 m with an average weight of around 2 kg. While in normal hovering mode, the main rotors induce momentum around the roll axis, while the auxiliary rotor is used for pitch control. Yaw control is enabled by aileron deflections. During transition flight , the main wing is rotated along the body fixed y-axis referred to as σ. In cruising configuration, the tilt wing aircraft is actuated like a conventional aircraft with aileron, elevator and thrust control. Differential trust is used as yaw-control.

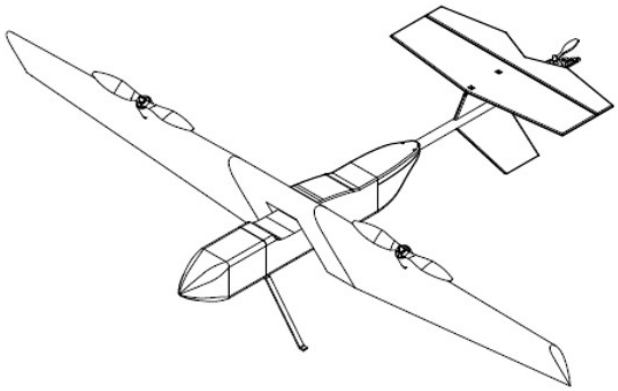

Figure 1: Exampled tilt wing in hover mode

	hover flight	emergency mode
asym. thrust δ_{asym}	roll	roll
tail rotor δ_{aux}	pitch	(-)
aileron ξ	yaw	yaw
elevator η	(-)	(-)
tiltrotor σ	(-)	pitch

Table 1: Actuators in hover flight and emergency mode

During tail rotor failure the attitude controller stabilizes the aircraft around the trimm state where the thrust vector points to earth centered -z_g. While in hover mode the motion of the aircraft can be described by the following set of equations:

$$\begin{bmatrix} \dot{u} \\ \dot{v} \\ \dot{w} \end{bmatrix} = \begin{bmatrix} \dot{u}' \\ \dot{v}' \\ \dot{w}' \end{bmatrix} + \begin{bmatrix} p \\ q \\ r \end{bmatrix} \times \begin{bmatrix} u \\ v \\ w \end{bmatrix} \tag{1}$$

$$\begin{bmatrix} \dot{u}' \\ \dot{v}' \\ \dot{w}' \end{bmatrix} = \begin{bmatrix} \frac{F_t \cdot cos(\sigma)}{m} - g \cdot sin(\Phi) - F_{aero_x} \\ g \cdot cos(\Theta) \cdot sin(\Phi) - F_{aero_y} \\ \frac{-F_t \cdot sin(\sigma)}{m} - g \cdot cos\Phi \cdot cos(\Theta) - F_{aero_z} \end{bmatrix} \tag{2}$$

$$\begin{bmatrix} \dot{p} \\ \dot{q} \\ \dot{r} \end{bmatrix} = I^{-1} \cdot \left[\begin{bmatrix} M_x \\ M_y \\ M_z \end{bmatrix} - \begin{bmatrix} p \\ q \\ r \end{bmatrix} \times \left(I \cdot \begin{bmatrix} p \\ q \\ r \end{bmatrix} \right) \right] \tag{3}$$

$$\begin{bmatrix} M_x \\ M_y \\ M_z \end{bmatrix} = \begin{bmatrix} M_{mot_x} + F_{ail} \cdot y_{cog} \cdot sin(\sigma) + M_{aero_x} \\ M_{mot_y} + M_{servo} + M_{aero_y} \\ M_{mot_z} + F_{ail} \cdot y_{cog} \cdot cos(\sigma) + M_{aero_z} \end{bmatrix} \tag{4}$$

$$\begin{bmatrix} M_{mot_x} \\ M_{mot_y} \\ M_{mot_z} \end{bmatrix} = \begin{bmatrix} F_{dt} \cdot y_{cog} \cdot cos(\sigma) \\ F_t \cdot z_{cog} \cdot cos(\sigma) + F_t \cdot x_{cog} \cdot sin(\sigma) \\ F_{dt} \cdot y_{cog} \cdot sin(\sigma) \end{bmatrix} \tag{5}$$

With $[\dot{u}\ \dot{v}\ \dot{w}]^T$ being the body fixed translation accelerations, $[\dot{p}\ \dot{q}\ \dot{r}]^T$ the body fixed rotational accelerations, the mass m of the aircraft, $I = [I_{xx}\ I_{yy}\ I_{zz}]^T$ inertia around the main body axes, F_t the main thrust of the front motors, F_{dt} the differential thrust between the left and right front motor, F_{ail} the force induced by deflection of the ailerons, $[F_{a_x}\ F_{a_y}\ F_{a_z}]$ aerodynamic forces, $[M_{aero_x}\ M_{aero_y}\ M_{aero_z}]$ aerodynamic moments, $[M_{mot_x}\ M_{mot_y}\ M_{mot_z}]$ motor induced moments, $[x_{cog}\ y_{cog}\ z_{cog}]^T$ being the pivot point of the wing-body and span-wise position of motors and ailerons.

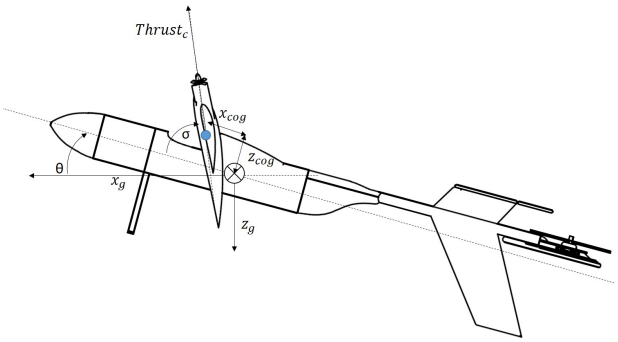

Figure 2: Model of the tilt wing aircraft during tail actuator failure

The aerodynamic effects are computed by breaking down the aircraft structure into aerodynamic plates and adding up the forces and momentum according to [4] . While the aerodynamic effects relative to the air are accounted for in M_{aero}, M_{servo} models the added moment due to the torque applied to the wing and therefore the equivalent reaction moment on the center of gravity:

$$M_{servo} = M_{rot} + I_{yy_{wing}} \cdot \ddot{\sigma} \tag{6}$$

By using a point mass model of the wing, we approximate the inertia $I_{yy_{wing}}$ of the wing and therefore account for the effects of angular acceleration $\ddot{\sigma}$.

M_{rot} accounts for the aerodynamic effects due to angular wing tilt velocity $\dot{\sigma}$. By separating the wing into aerodynamic plates above and below the wing pivot point, we are able to derive equations for the aerodynamic forces acting on the wing.

$$M_{rot} = F_1 \cdot \frac{t_1}{2} + F_2 \cdot \frac{t_2}{2} \tag{7}$$

By modeling our aerodynamic elements as plates with span wise length $b = 1.5\ m$, root wise length t and drag coefficient $c_d = 1.2$ and assuming the main drag forces acting on the center of each plate, we can calculate each force as

$$F = c_d \cdot \frac{\rho}{2} \cdot \dot{\sigma}.^2 \cdot t^3 * b \tag{8}$$

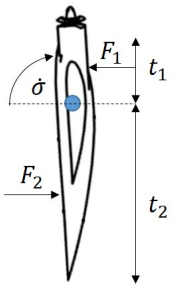

Figure 3: Modeling of the aerodynamic effects due to a change in σ

2.1 Trimm state in emergency mode

Modeling the aircraft as a point mass and neglecting aerodynamic forces due to small rotational velocity, the system can be described around the pitch axes as a pendulum with longitudinal movement. While the thrust generated by the two main rotors is needed to counteract gravitational forces, momentum is generated around the pitch axis. During tail rotor recovery, the body swings beneath the wing pivot point in a rear centered cog while the main thrust vector is used for stabilization and height control. The aircraft which is being

stabilized has a rear centered center of gravity (cog). While a cog below the wing pivot would lead to a neutral moment and therefore enable the aircraft to hover vertical with respect to the body angle θ, a rear centered cog was chosen to increase the margin for a shift of cog due to added mass in front of the designed cog. The main advantage of a rear centered cog in contrast to a forward centered cog is a lift contribution of the tail rotor in normal mode. Figure 4 depicts the time frame recovery phase of the aircraft under tail rotor failure.

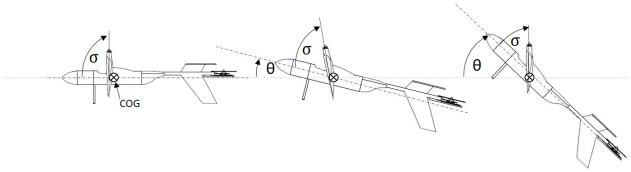

Figure 4: Movement of the aircraft during recovery

3 CONTROL STRATEGY

In this chapter we will discuss the overall control strategy and give more insight to the separate controllers and control allocation. To stabilize the unmanned aircraft under tail-rotor failures the following control structure is employed:

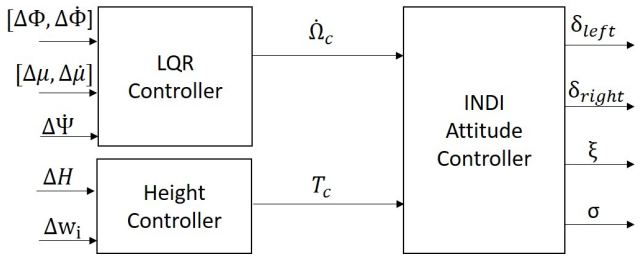

Figure 5: Control structure

The controller depicted in this paper is part of an cascaded controller loop. In the inner controller loop an INDI attitude controller is employed. The INDI attitude controller's task is to stabilizes the aircraft in normal and emergency mode by using body fixed angular acceleration $\dot{\Omega}_c$ and Thrust command T_c as input and actuator commands described in table 1 as output. To achieve this dual purpose task an fault detection system and emergency moding system is employed to redesign the INDI controller by adjusting the actuator effectivity matrix B. During tail rotor-failure, a PD height controller is employed to generate a thrust command T_c according to the height and inertial velocity deviations ΔH and Δw_i. Angular acceleration commands $\dot{\Omega}_c$ are generated by separate LQR based acceleration controllers which use the deviations of roll angle $\Delta\Phi$ with rate feedback, thrust angle $\Delta\mu$ with rate feedback and yaw velocity $\Delta\dot{\Psi}$ respectfully. Further details regarding the controller parts are depicted in the following subsections.

3.1 Incremental Nonlinear Dynamic Inversion

The concept of Incremental Nonlinear Dynamic Inversion (INDI) has already been discussed in several papers [5] [6] and will not be explained in detail. The basic concept of INDI is to invert the plant dynamics and therefore shape the closed-loop dynamics as a series of integral states. A simple derivation of the INDI control law is as follows.

$$\dot{x} = f(x) + g(x) \cdot u \tag{9}$$

Equation 9 represents the formulation of a multi input multi output (mimo) system. f represents the effects of aerodynamic and flight dynamic characteristics affecting the aircraft. g models the effects of input vectors on the system. By inverting equation 9 we gain:

$$u = g(x)^{-1} \cdot (\dot{x} - f(x)) \tag{10}$$

This control law enables the transformation from the current system state to an desired system state by controlling the state input u. The downside for this simple approach is the needed modeling effort around the mostly unknown aerodynamic effects in $f(x)$. To reduce the modeling effort, [5] [7] propose an incremental dynamic approach by employing a taylor series around the state vector x and input vector u. This approach reduces the impact of model mismatches and therefore aerodynamic effects are compensated.

The resulting governing control law for a rotational incremental nonlinear dynamic inversion is depicted in the following equation:

$$\Delta u = B^{-1} \cdot I \cdot (\dot{\Omega}_c - \dot{\Omega}) \tag{11}$$

where B is the inverted actuator effectivity matrix with their associated dynamics, I the moment of inertia and $\delta(\dot{\Omega})$ the difference between commanded and measured angular accelerations. The governing control law therefore computes incremental steps on the actuators command to transfer the system from the current rotational state to an desired rotational state.

3.2 Angular acceleration controller

In this chapter we will describe the development and implementation of an LQR-based angular acceleration controller. This angular acceleration controller uses the angle deviation of a controlled trim state as input. The basic principle of LQR control is to minimize a cost function designed with weighting factors either by prioritizing state variables or actuator usage. The cost-function in time discrete finite horizon formulation is depicted in equation 12.

$$J = x_N^T \cdot Q \cdot x_N + \sum_{k=0}^{N-1} (x_k^T \cdot Q \cdot x_k + u_k^T \cdot R \cdot u_k + 2 \cdot x_x^T \cdot N \cdot u_k) \tag{12}$$

Q and R are positive, symmetric weighting factors prioritizing either state error variables x or actuator input u. By minimizing the quadratic cost function depicted in equation 12, a feedback control law can be developed to minimize state error:

$$u = -K_{LQR} \cdot x \tag{13}$$

By implementing a time-discrete LQR-controller, we can model reaction times concerning actuator dynamics and computational time. Study's on our flight controller and flight data have shown, that a time delay of $\delta t = 7 \cdot controller_{freq.}$ occurs. Due to the principle of INDI inverting the plant dynamics, we are able to develop a linear model of our plant by modeling our INDI attitude controller as a transfer function of first order with a time constant of $T_{INDI} = 0.1$ and a time delay of $t_{delay} = 0.035s$. To account for the time delay we need to extend our classical model of linear state space with additional time delayed state variables and extended matrixes as depicted as follows:

$$\begin{aligned} \dot{x}_{n+1} &= A \cdot x_n + B \cdot u_n \\ y_n &= C \cdot x_n + D \cdot u_n \end{aligned} \tag{14}$$

Depicted in equation 14 is the linear state space model around our body fixed pitch axis consisting of an extended state vector $x_n = [\mu_n \; \dot{\mu_n} \; \ddot{\mu_n} \cdots \ddot{\mu}_{n-7}]^T$,terestrial based indi input $u = (\dddot{\mu_c})$ extended system matrix $A \in R^{10x10}$ extended input matrix $B \in R^{10x1}$, extended output matrix $C \in R^{10x10}$ and feedthrough matrix $D = 0$. While μ and $\dot{\mu}$ are measurable state variables, states regarding $[\ddot{\mu}_n, ...\ddot{\mu}_{n-7}]^T$ need to be estimated. Assuming our INDI model representation is correct, we are able to construct an linear observer model which uses $\ddot{\mu_c}$ as input and estimates $x_{n_{observer}} = [\dddot{\mu_n} \; \ddot{\mu}_{n-1} \; ... \; \ddot{\mu}_{n-7}]^T$. By using the transformation matrix M_{bi} from terrestrial to the body fixed frame, we are able calculate an angular pitch acceleration $\dot{q_c}$ for the INDI attitude controller

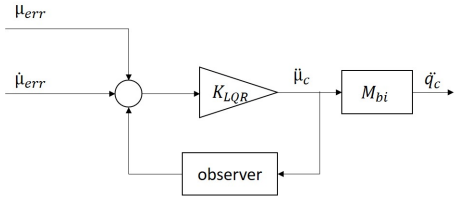

Figure 6: LQR Controller

3.3 Height controller

Task of the height controller is at first to maintain altitude during tail actuator failure recovery. Once a steady state attitude is reached, a controlled descend is initiated. To achieve this goal, a force F_z is generated by a PD controller which acts contrary to the gravitational forces along the z_g axis.

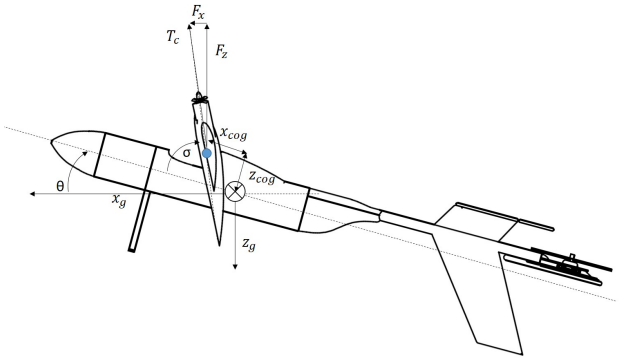

Figure 7: Height control

By considering equation 15 we can calculate a Thrust command T_c depending on the pitch θ and tilt angle σ of the aircraft.

$$T_c = \frac{F_z}{sin(\sigma + \theta)} \tag{15}$$

3.4 Actuator modeling

The control law depicted in equation 11 uses the inverted model of actuators to form an inner control loop. The actuator models consist of static and dynamic properties and describe the change in momentum due to changes in the actuator deflection. As mentioned in [8], the actuator modeling affects the closed-control loop dynamics and can be modeled as a compromise between controller dynamics and modeling effort. In this paper we only adress extensions to the actuator modeling as described by [6] regarding the pitch authority.

As depicted in equation 3 the influence of a deviation of σ or T lead to a pitching moment. In this chapter we will describe the contribution of a tilting motion of the main wing and thrust to the pitching moment. By partial differentiating equation 3 with respect to σ, we can express the influence of σ:

$$\frac{\delta M}{\delta \sigma} = x_{COG} \cdot cos(\sigma_0) \cdot F_{main} - F_{main} \cdot z_{COG} \cdot sin(\sigma_0) \tag{16}$$

where σ_0 denote the tilt angle in the previous controller time step and F_{main} is the current thrust approximated by the following motor model:

$$F_t = (V_{Bat} \cdot K_{Bat} - K_{offset}) \cdot \delta^2 \tag{17}$$

where V_{Bat} is the measured supply voltage, $\delta \in [0...1]$ the normalized throttle signal, K_{Bat} and K_{offset} modeling parameters derived from experimental data. By adding up the modeled thrust for the left and right motor we are able to calculate the main thrust acting on the tilt wing aircraft in near stationary flight.

$$F_{main} = F_{t_{left}} + F_{t_{right}} \tag{18}$$

As for the dynamic model of our servo, we employed a non-linear model consisting of a time delay of $t_{delay} = 0.035s$,and rate limit corresponding to the data from our test bench [8].Assuming the servo velocity acts instantaneous with the maximum velocity we are able to model $\dot{\sigma}$ and $\ddot{\sigma}$. The influence of a thrust change on the pitch momentum can be modeled similar to the modeling of the wing tilt effects. By differentiating equation 3 with respect to F_t we can derive the following equation:

$$\frac{\delta M}{\delta_\delta} = (x_{COG} \cdot sin(\sigma_0) - \cdot z_{COG} \cdot cos(\sigma_0)) \cdot \frac{\delta_{F_t}}{\delta_\delta} \tag{19}$$

where σ_0 is the previous wing angle and $\frac{\delta_{F_t}}{\delta_\delta}$ the derivative of equation 15 with respect to δ.

4 Simulation and Results

To validate our controller design presented in the previous chapters, we will conduct simulation studies with regard to the area of application for our emergency mode and controller performance.

4.1 Controller performance during attitude recovery

To evaluate our controller and get a first understanding of the motion of the modeled aircraft, we simulated an tail rotor failure by deactivating tail- thrust in our aircraft plant at a given time $t_{failure}$. Due to the lack of tail thrust, emergency mode was activated and the attitude controller stabilizes the aircraft. Initial setup is a hover flight with $[u_g\ v_g\ w_g] = [0\ 0\ 0]\frac{m}{s}$, $[\phi\ \mu\ \psi] = [0\ 90\ 0]^\circ$ and no wind speed $V_w = 0\ \frac{m}{s}$.

Figure 8 shows the translation movement and angles during hover and tail rotor failure recovery. Until reaching the failure time $t_{failure} = 7s$ the modeled aircraft remains in steady hover flight where the inertial velocities remain near 0. By deactivating the tail thrust, θ starts to increase while the wing-tilt angle σ decreases at maximum speed to stabilize the aircraft around its trim state. At the time $t = 12s$ a steady flight is achieved.

Figure 9 shows the attitude LQR controller performance during tail rotor recovery. In general the performance of the LQR controller with regard to thrust angle μ compared to yaw or roll commands can be considered sluggish. This is due to a relative large difference between θ_{start} and θ_{trimm} and a compromise between attitude angles and angular velocities. Studies regarding over prioritization of angle commands have shown an increasing overshoot of the commanded trim angle.

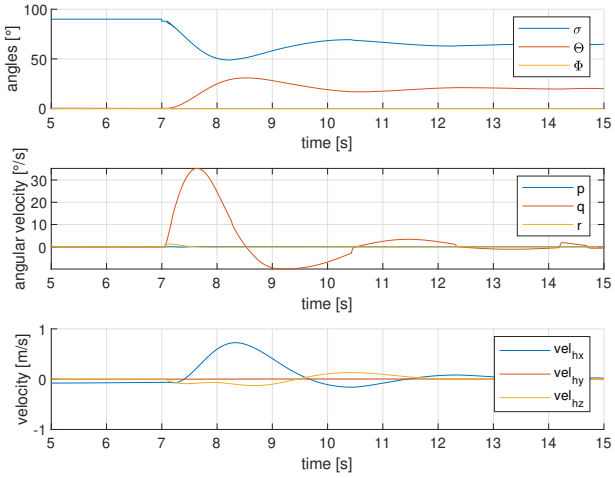

Figure 8: Motion of the aircraft during tail rotor recovery

This is due to the increased induced momentum generated by thrust. On the other side a over prioritization of pitch damping resulted in an increasing height loss and longitudinal acceleration.

By using our closed loop dynamic model of our tilt servo we are able to obtain expected accelerations regarding our pitch axis. By filtering the commanded angular accelerations, we are able to asses the performance of our INDI inner control loop. Figure 10 shows exemplary the INDI time series with our expected $\dot{q}_c$ and measured $\dot{q}$. We can see that around $t_{failure} = 7s$ our INDI model mismatches our measured angular accelerations. The main cause for the model mismatch are aerodynamic moments which are not modeled in the INDI controller. Studies have shown, that during recovery, the longitudinal aerodynamic velocity buildup leads to an pitch moment due to aerodynamic forces acting above the cog.

Figure 11 shows the deviation of a commanded height including horizontal velocities during tail rotor recovery. The horizontal coordinate system composes the terrestrial fixed velocities vel_g transferred to the horizontal system vel_h by angle ψ. The overall performance of the controller regarding a height loss during tail rotor recovery is very satisfactory. As mentioned before, our developed emergency mode is a compromise between height loss and longitudinal velocity buildup with a prioritization on reduction of uncontrolled height loss. While the height loss is minimal $\Delta H = 0.25\ m$, a longitudinal velocity buildup $u_h = 0.9\ m/s$ and following reduction can be observed.

To investigate the controller performance based on the initial attitude, simulations with deviating starting attitudes have been performed. Figure 12 shows exemplary the attitude performance of the controller. In this setup stationary flights with deviating roll angles ϕ have been performed. At

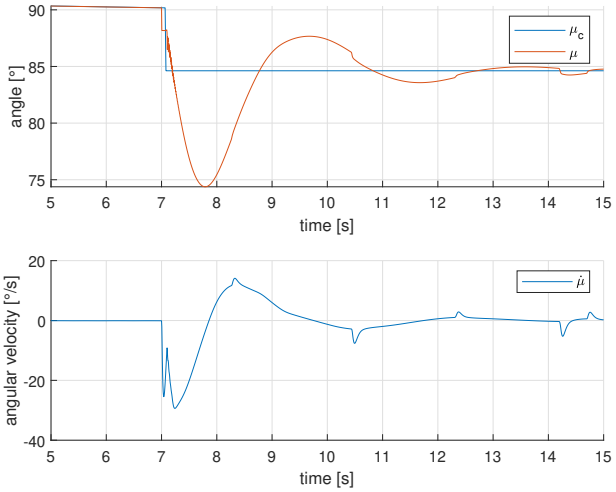

Figure 9: Attitude control performance during tail rotor failure recovery

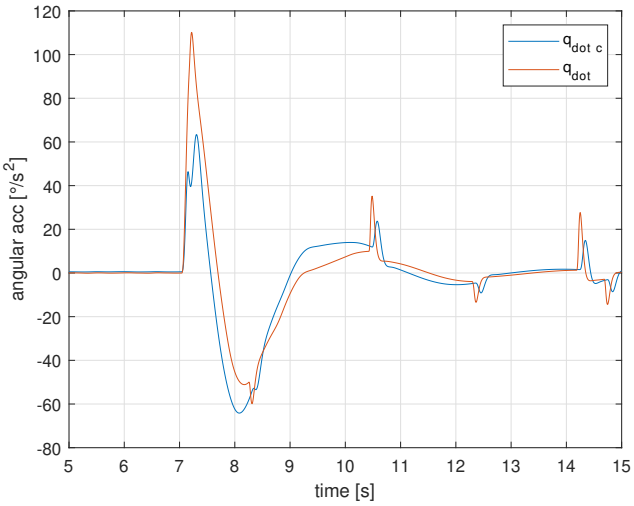

Figure 10: INDI controller performance

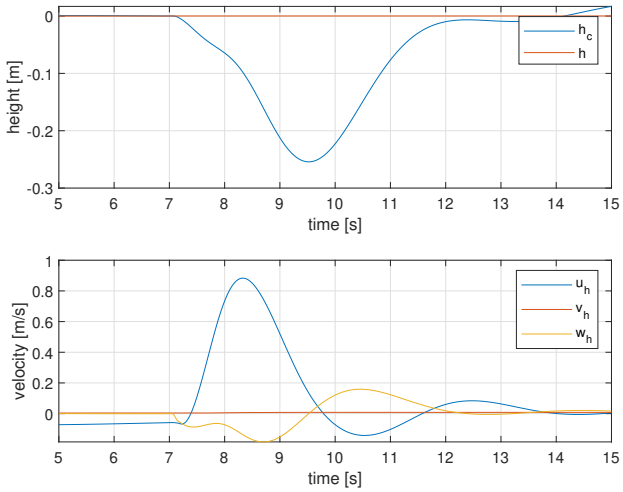

Figure 11: Height loss during emergency recovery

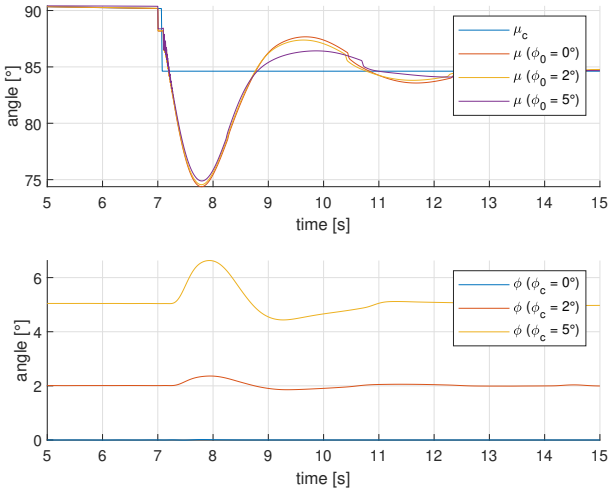

Figure 12: Attitude controller performance based on initial attitude

$t_{failure} = 7s$ emergency mode was activated and a tail rotor recovery was performed. While increasing initial roll angles lead to a larger deviation in ϕ, μ is largely unaffected. Roll angles above $\phi > 7$ have shown an insufficient heading control due to actuator saturation. This can be traced back to aerodynamic forces acting on the vertical stabilizer resulting from lateral velocity $v_{yh} = 6.5\ m/s$ which is considered an unrealistic flight state. Studies regarding initial $\dot{\psi}$ have shown similar results.

4.2 *Maneuverability in stabilized mode*

To evaluate the performance and boundary's of the emergency controller we applied step and ramp responses after the recovery from a tail rotor failure around the pitch and roll axis. As we can see in figure 13, the overall performance of the controller during a step response is acceptable. While the pitch controller can still be considered sluggish although not as sluggish during tail rotor compensation, roll is considered good.

By analyzing a ramp response of our controller we are able to evaluate a steady state reaction of our system regarding actuator behavior and saturation effects. Figure 14 shows a near steady state reaction where the pitch angle μ is reduced from stationary state. With a decreasing thrust angle μ, wing angle σ is decreased as well while the body pitch angle θ increases. The reason for this is still under investigation but

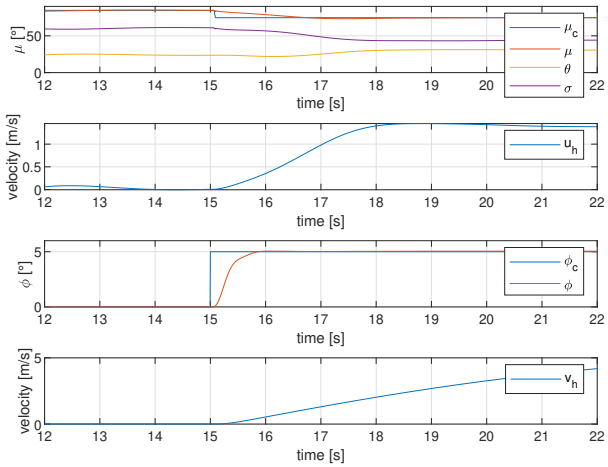

Figure 13: Step responses around roll and pitch

is most likely attributed to the overall aerodynamic effects acting on the aircraft. With further decreasing σ, θ starts to decrease as well, which is due to the overall influence of the motor thrust acting on the cog. At around $t = 47s$ σ starts to oscillate with a high frequency. Studies regarding the INDI indicate that modeling errors occur and need to be further investigated.

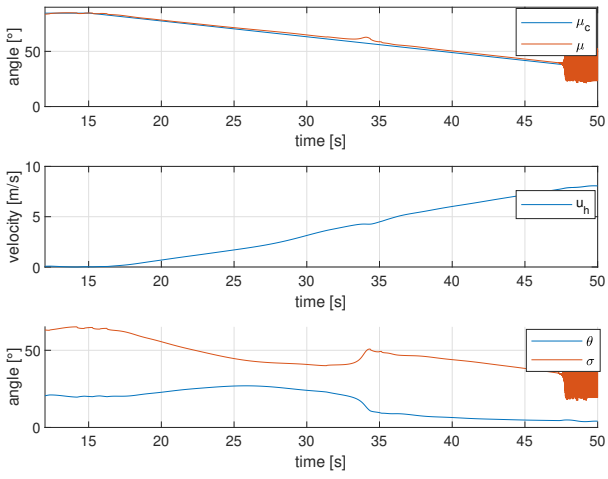

Figure 14: Ramp response around pitch axis.

Generally we are able to control our aircraft in emergency mode around all axis. By influencing our thrust vector, we are able to induce force and build up horizontal velocities. By analyzing our height controller it became obvious, that a steady descent and climb is achievable while still being stabilized.

4.3 *Controller performance under wind effects*

In this chapter we will analyze the robustness of our proposed control structure during the transition phase from normal to emergency mode. We will put our emphasis on the effects of wind gust and wind speeds ranging from expected wind speeds of $u_{hw} = [0...10]\ \frac{m}{s}$. To evaluate our controller performance with regard to wind effects, we employed a wind model with averaged wind and gustiness. The task of the aircraft is to remain stationary in terms of terrestrial velocities. Therefore we expanded our control structure by implementing a PI controller with input Δu_h being the deviation of inertial longitudinal velocity and output the thrust pitch angle μ for longitudinal motion control.

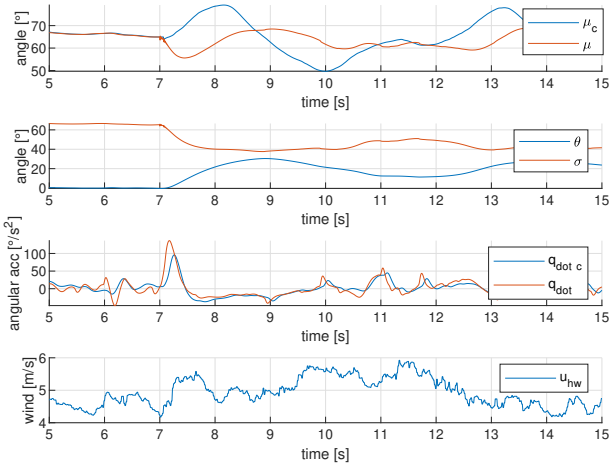

Figure 15: Controller performance under wind effects

Figure 15 displays exemplary the performance of the controller under wind effects at speeds $u_{hw} = 5\ \frac{m}{s}$. Although the controller is rather sluggish around its pitch axis we are able to maintain stationary in the context of terrestrial velocities until $u_{hw} = -u_a = 7\frac{m}{s}$. When exceeding $u_{hw} > 7$ oscillations similar to figure 14 occurred. Studies related to 4.1 and 4.2 under wind effects have shown similar performance.

5 CONCLUSION AND FUTURE WORK

In this work we presented an alternative approach to increase safety of unmanned aerial vehicles by employing an emergency mode to compensate for tail rotor failures rather than redundant design concepts. The proposed control structure transforms an tilt wing aircraft with 3 motors into an basic flying wing. We employed a robust INDI controller combined with an LQR attitude controller and height control. Simulation studies have shown, that our aircraft was able to stabilize after tail rotor failure under different wind and starting attitude conditions. While height loss was minimal, we encountered longitudinal accelerations, which lead

to forward and backward movement. This effect was considered adequate as a primary object of the proposed control structure was to reduce the risk of ground damage and a appropriate horizontal airspace around our aircraft is available. We were able to induce force for a controlled flight and therefore enable an controlled flight after tail rotor failure. The overall controller performance was acceptable while the pitch authority remains sluggish. Future work will concentrate on the improvement of pitch control. Particularly the compromise between angular damping and angular commands will be further analyzed. Furthermore test flights in an controlled flight space are performed.

REFERENCES

[1] Hamidreza Jafarnejadsani Donglei Sun Florian Holzapfel Xiang Fang, Neng Wan and Naira Hovakimyan. Emergency landing trajectory optimization for fixed-wing uav under engine failure. 2019.

[2] G. Narvydas R. Maskeliūnas R. Damaševičius B. AL-Madani, M. Svirskis. Design of fully automatic drone parachute system with temperature compensation mechanism for civilian and military applications. *Journal of advanced Transportation*, 2018.

[3] R. Isermann. *Fault- Diagnosis Systems*. Springer Science and Business Media, LLC, Heidelberg, GER, 2006.

[4] P. Hartmann. Vorausschauende flugbahnregelung fuer kippfluegelflugzeuge. 2017.

[5] J.A. Mulder S. Sieberling, Q.PChu. Robust flight control using incremental nonlinear dynamic inversion and angular acceleration prediction. *Journal of Guidance, Control, and Dynamics*, 33(6), 2010.

[6] F. Binz T.Islam, D. Moormann. Attitude control of tiltwing aircraft using a wing-fixed coordinate system and incremental nonlinear dynamic inversion. In *IEEE International Micro air vehicle conference and competition (IMAV)*, 2018.

[7] J. A. Mulder R. R. da Cosat, . P. Chu. Reentry flight controller design using nonlinear dynamic inversion. *Journal of Spacecraft and Rockets*, 40(1), 2003.

[8] F. Binz D. Moormann. Actuator modeling for attitude control using incremental nonlinear dynamic inversion. In *IEEE International Micro air vehicle conference and competition (IMAV)*, 2019.